Archives of Hydro-Engineering and Environmental Mechanics
Vol. 52 (2005), No. 4, pp. 351–371

Investigations of Shear Localization in Granular Bodies within an Anisotropic Micro-Polar Hypoplasticity

Jacek Tejchman

Faculty for Civil and Environmental Engineering, Gdańsk University of Technology,
ul. Narutowicza 11/12, 80-952 Gdańsk, e-mail: tejchmk@pg.gda.pl

(Received September 29, 2005; revised December 31, 2005)

Abstract

The paper focuses on the numerical analysis of the effect of texturial anisotropy on shear localization in cohesionless granular materials. For simulation of the mechanical behavior of a granular material during a monotonous deformation path, a hypoplastic constitutive model was used. To take into account a characteristic length of micro-structure, the constitutive model was extended by micro-polar terms. To take into account texturial effects, the granular hardness was modified. The calculations were carried out with a sand specimen during plane strain compression under constant lateral pressure. A stochastic and uniform distribution of the initial void ratio in the granular specimen was assumed. In addition, shear localization for two different uniform initial void ratios was investigated.

Key words: bedding plane, granular material, hypoplasticity, micro-polar theory, shear zone, texturial anisotropy

1. Introduction

Granular materials build discrete systems composed of grains of different shape, size, roundness and roughness. Thus, their behaviour is strongly anisotropic and influenced by the orientation of grains (fabric) with respect to the loading direction (Boehler and Sawczuk 1977, Kanatani 1984, Oda et al 1985, Khidas and Jia 2005). This inherent anisotropy due to fabric (texture) is called a transverse isotropy since the material has a rotational symmetry with respect to one of the co-ordinates' axes. The plane perpendicular to the orientation direction is called bedding plane and is a plane of isotropy.

The laboratory experiments show that the orientation of the bedding plane relative to the principal stress directions has a pronounced effect on the stress-strain behaviour (Arthur and Phillips 1975, Lam and Tatsuoka 1988, Tatsuoka et al 1990, 1991, 1994, 1997, Abelev and Lade 2003). The material stiffness, peak friction angle and average volume change are higher and strain corresponding to the

peak friction angle is smaller for loading perpendicular to the bedding plane than for loading parallel to it. The inclination of the shear zone with respect to the bottom becomes smaller (Abelev and Lade 2003). For large monotonic shearing, the stress ratio approaches a stationary value (Yamada and Ishihara 1979, Tatsuoka et al 1994), i.e. anisotropy vanishes at critical state due to a so-called SOM-effect (swept out of memory effect) (Gudehus 1997). The DEM simulations (Pena et al 2005) confirm also this important property of granular bodies.

For describing the behaviour of granular materials within continuum mechanics, mainly elasto-plastic constitutive (Lade 1977, Vermeer 1982, Pestana and Whittle 1999) and hypoplastic constitutive models (Kolymbas 1977, Gudehus 1996, Bauer 1996, Chambon 2001, Lanier et al 2004) are applied. To describe the shear zone formation (thickness, inclination and spacing), these approaches have to be enriched by a characteristic length of microstructure by means of a micro-polar (Mühlhaus 1990, Tejchman and Gudehus 2001, Maier 2002, Gudehus and Nübel 2004), non-local (Pijaudier-Cabot and Bazant 1987, Maier 2002, Tejchman 2004), second-gradient theory (Aifantis 1984, de Borst and Mühlhaus 1992, Sluys 1992, Pamin 1994) and viscosity (Loret and Prevost 1990, Sluys 1992, Lodygowski and Perzyna 1997). Due to the presence of a characteristic length of micro-structure, the approaches regularize the ill-posedness i.e. preserve the well-posedness of the underlying incremental boundary value problem caused by strain-softening material behaviour and localization formation (differential equations of motion do not change their elliptic type during quasi-static calculations and hyperbolic type during dynamic calculations) and prevent pathological discretization sensitivity (de Borst et al 1992). Thus, objective and properly convergent numerical solutions for localized deformation (mesh-insensitive load-displacement diagram and mesh-insensitive deformation pattern) are achieved. Another numerical technique which enables to remedy the drawbacks of standard FE-methods and to obtain mesh-independent results during the description of the formation of shear zones is the so-called strong discontinuity approach affording a finite element with a displacement discontinuity (Larsson and Larsson 2000, Regueiro and Borja 2001).

There exist two models in hypoplasticity to describe textural anisotropy. The first one was suggested by Bauer et al (2004) wherein a structure tensor was included taking into account the space orientation of the bedding plane. The concept follows the idea of Boehler and Sawczuk (1977) for plasticity. The structural tensor influences the nonlinear part of the hypoplastic equation in such a way that the strength increases for the major normal stress perpendicular to the bedding plane. This effect disappears at critical state. The anisotropic model requires actually 2 additional material parameters which have the form of an exponential function. The calculations with a gradient hypoplastic constitutive law (Tejchman et al 2006) show that the model can realistically describe a decrease of the initial stiffness, peak internal friction angle and volume change, and an increase of the strain corresponding to the peak friction angle during plane strain compression

test involving shear localization. The disadvantage of the model is the fact that the material parameters have no physical meaning and the model is not able to predict anisotropy if the initial void ratio is equal to the critical one. In turn, the second model was proposed by Niemunis (2003) wherein the initial critical void ratio was modified depending on the orientation of stress to the bedding plane. Thus, the density factor increased the strength and volume change for loading perpendicular to the bedding plane. The advantage of the model is the possibility to impose anisotropy for all densities. The model has also two additional constants. The calculations with a micro-polar hypoplastic constitutive law (Tejchman and Niemunis 2005) show that the model can realistically describe a decrease of the initial stiffness, peak internal friction angle and volume change during plane strain compression test involving shear localization. However, the vertical strain corresponding to the peak friction angle during a plane strain compression test with shear localization is almost independent of the bedding orientation. In both anisotropic hypoplastic models, the critical state line remains unique and isotropic.

In the paper, the effect of the orientation of the bedding plane on a spontaneous shear zone formation in initially cohesionless sand during plane strain compression under constant lateral pressure was numerically investigated with the finite element method and a micro-polar hypoplastic constitutive model (Tejchman et al 1999, Tejchman 2004) which is able to describe the essential properties of granular bodies during shear localization in a wide range of pressures and densities during monotonous deformation paths. To simulate anisotropic effects due to texture and to avoid some disadvantages of existing anisotropic hypoplastic models (Niemunis 2003, Bauer et al 2004), one hypoplastic material parameter, namely granular hardness, was slightly modified. The calculations were carried out with a uniform and stochastic distribution of the initial void ratio.

2. Experiments

Comprehensive laboratory experiments on the effect of texturial anisotropy were performed for plane strain compression by Tatsuoka et al (1994). The tests were carried out mainly with Silver Leighton Buzzard sand composed of sub-round grains (mean grain diameter $d_{50} = 0.62$ mm, non-conformity coefficient $U_c = 1.11$). The specimen was 20 cm long and 8 cm wide. The confining platens were very smooth. Dense specimens with a void ratio of about $e_0 = 0.55$ were prepared. Several different angles δ were employed between the pouring direction and the direction of the minor principal stress (Fig. 1). The angle δ was the angle of the direction of the major principal stress relative to the bedding plane direction. The specimen was wetted, frozen, thawed and re-dried. Fig. 2 presents the relationships among the stress ratio σ_1/σ_3, the average shear strain $\gamma = \varepsilon_1 - \varepsilon_3$ and the average volumetric strain $\varepsilon_v = \varepsilon_1 + \varepsilon_3$ for different angles of δ between 90 and 0 degrees at $\sigma_3 = 80$ kPa (for dense SLB sand with $e_0 = 0.555$–0.563).

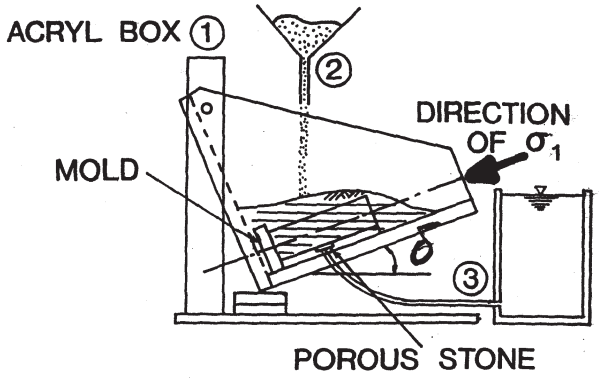

Fig. 1. Method used to prepare sand specimens (Tatsuoka et al 1994)

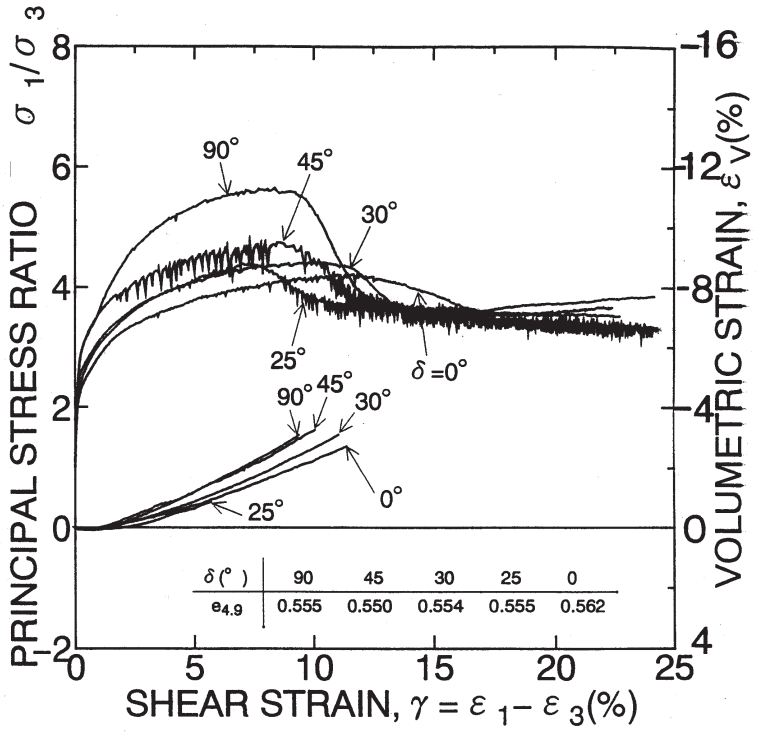

Fig. 2. Relationships among the stress ratio σ_1/σ_3, the average shear strain $\gamma = \varepsilon_1 - \varepsilon_3$ and the average volumetric strain $\varepsilon_v = \varepsilon_1 + \varepsilon_3$ for different angles of δ between 90 and 0 degrees at $\sigma_3 = 80$ kPa (Tatsuoka et al 1994)

The experimental peak internal friction angle calculated by the Mohr's formula with the aid of principle normal stresses increases with increasing angle δ, and is: $\phi_p = 39.6^\circ$ ($\delta = 0^\circ$), $\phi_p = 40.0^\circ$ ($\delta = 25^\circ$), $\phi_p = 42.0^\circ$ ($\delta = 45^\circ$), $\phi_p = 43.9^\circ$ ($\delta = 65^\circ$) and $\phi_p = 45.1^\circ$ ($\delta = 90^\circ$), respectively. Thus, the peak friction angle increases by about 10% with decreasing δ. The peak friction angle is reached for the shear strain $\gamma = 6$–10% which increased as δ decreased (in particular for $\delta < 45^\circ$). The residual friction angle is about 25.5°. The average global dilatancy angle increases with increasing angle δ.

3. Micro-Polar Hypoplastic Model for Isotropic Materials

To describe shear localization, a non-polar hypoplastic constitutive law proposed by Gudehus (1996) and Bauer (1996) for monotoneous deformation paths was extended by means of a micro-polar continuum (Mühlhaus 1990). Each material point has for the case of plane strain, three degrees of freedom: two translational degrees of freedom and one independent rotational degree of freedom. The gradients of the rotation are connected to curvatures which are associated with couple stresses. It leads to non-symmetry of the stress tensor and the presence of a characteristic length.

A micro-polar hypoplastic constitutive law describes the evolution of stresses and couple stresses depending on the current void ratio, stress and couple stress state and rate of deformation and curvatures. Due to the incremental non-linearity with the rate of deformation and curvature, it is able to describe both a non-linear stress-strain and volumetric behaviour of granular bodies during shearing up to and after the peak with two single tensorial equations. It includes also: barotropy (dependence on pressure level), pycnotropy (dependence on density), dilatancy and contractancy and material softening during shearing of a dense material. In contrast to elasto-plastic models, a decomposition of deformation components into elastic and plastic parts, the formulation of a yield surface, plastic potential, flow rule and hardening rule is not needed. The feature of the model is a simple formulation and procedure for determination of material parameters with standard laboratory experiments (Herle and Gudehus 1999). The parameters are directly related to granulometric properties encompassing grain size distribution curve, shape, angularity and hardness of grains. The constitutive law can be summarized for plane strain as follows (Tejchman 2004, Tejchman and Bauer 2005):

$$\overset{o}{\sigma}_{ij} = f_s \left[L_{ij}\left(\hat{\sigma}_{kl}, \hat{m}_k, d^c_{kl}, k_k d_{50}\right) + f_d N_{ij}\left(\hat{\sigma}_{ij}\right) \sqrt{d^c_{kl} d^c_{kl} + k_k k_k d^2_{50}} \right], \qquad (1)$$

$$\overset{o}{m}_i / d_{50} = f_s \left[L^c_i\left(\hat{\sigma}_{kl}, \hat{m}_k, d^c_{kl}, k_k d_{50}\right) + f_d N^c_i\left(\hat{m}_i\right) \sqrt{d^c_{kl} d^c_{kl} + k_k k_k d^2_{50}} \right], \qquad (2)$$

$$L_{ij} = a_1^2 d_{ij}^c + \hat{\sigma}_{ij} \left(\hat{\sigma}_{kl} d_{kl}^c + \hat{m}_k k_k d_{50} \right), \tag{3}$$

$$L_i^c = a_1^2 k_i d_{50} + a_1^2 \hat{m}_i \left(\hat{\sigma}_{kl} d_{kl}^c + \hat{m}_k k_k d_{50} \right), \tag{4}$$

$$N_{ij} = a_1 \left(\hat{\sigma}_{ij} + \hat{\sigma}_{ij}^* \right), \tag{5}$$

$$N_i^c = a_1^2 a_c \hat{m}_i, \tag{6}$$

$$\hat{\sigma}_{ij} = \frac{\sigma_{ij}}{\sigma_{kk}}, \tag{7}$$

$$\hat{m_i} = \frac{m_i}{\sigma_{kk} d_{50}}, \tag{8}$$

$$\overset{\circ}{\sigma}_{ij} = \overset{\bullet}{\sigma}_{ij} - w_{ik}\sigma_{kj} + \sigma_{ik} w_{kj}, \tag{9}$$

$$\overset{\circ}{m}_i = \overset{\bullet}{m}_i - 0.5 w_{ik} m_k + 0.5 m_k w_{ki}, \tag{10}$$

$$d_{ij} = \left(v_{i,j} + v_{j,i} \right)/2, \quad w_{ij} = \left(v_{i,j} - v_{j,i} \right)/2, \tag{11}$$

$$d_{ij}^c = d_{ij} + w_{ij} - w_{ij}^c, \quad k_i = w_{,i}^c, \tag{12}$$

$$w_{kk}^c = 0, \quad w_{21}^c = -w_{12}^c = w^c, \tag{13}$$

$$\overset{\bullet}{e} = (1 + e)\, d_{kk}, \tag{14}$$

$$e_i = e_{i0} \exp\left[- \left(-\sigma_{kk}/h_s \right)^n \right], \tag{15}$$

$$e_d = e_{d0} \exp\left[- \left(-\sigma_{kk}/h_s \right)^n \right], \tag{16}$$

$$e_c = e_{c0} \exp\left[- \left(-\sigma_{kk}/h_s \right)^n \right], \tag{17}$$

$$f_s = \frac{h_s}{n h_i} \left(\frac{1 + e_i}{e_i} \right) \left(\frac{e_i}{e} \right)^{\beta} \left(- \frac{\sigma_{kk}}{h_s} \right)^{1-n}, \tag{18}$$

$$h_i = \frac{1}{c_1^2} + \frac{1}{3} - \left(\frac{e_{i0} - e_{d0}}{e_{c0} - e_{d0}} \right)^{\alpha} \frac{1}{c_1 \sqrt{3}}, \tag{19}$$

$$f_d = \left(\frac{e - e_d}{e_c - e_d} \right)^{\alpha}, \tag{20}$$

$$a_1^{-1} = c_1 + c_2 \sqrt{\overset{\wedge}{\sigma}{}^{*}_{kl} \overset{\wedge}{\sigma}{}^{*}_{kl}} \left[1 + \cos(3\theta) \right], \tag{21}$$

$$\cos(3\theta) = -\frac{\sqrt{6}}{\left[\overset{\wedge}{\sigma}{}^{*}_{kl} \overset{\wedge}{\sigma}{}^{*}_{kl} \right]^{1.5}} \left(\overset{\wedge}{\sigma}{}^{*}_{kl} \overset{\wedge}{\sigma}{}^{*}_{lm} \overset{\wedge}{\sigma}{}^{*}_{mk} \right), \tag{22}$$

$$c_1 = \sqrt{\frac{3}{8}} \frac{(3 - \sin\phi_c)}{\sin\phi_c}, \quad c_2 = \frac{3}{8} \frac{(3 + \sin\phi_c)}{\sin\phi_c}, \tag{23}$$

wherein

- σ_{ij} – Cauchy stress tensor,
- σ^{*}_{ij} – deviatoric part of σ_{ij},
- $\overset{o}{\sigma}_{ij}$ – Jaumann stress rate tensor (objective stress rate tensor),
- m_i – Cauchy couple stress vector,
- $\overset{o}{m}_i$ – Jaumann couple stress rate vector (objective couple stress rate vector),
- e – current void ratio,
- d_{kl} – rate of deformation tensor (stretching tensor),
- w_{ij} – spin tensor,
- v – material velocity,
- d^{c}_{ij} – polar rate of deformation tensor,
- k_i – rate of curvature vector,
- w^{c} – rate of Cosserat rotation,
- f_s – stiffness factor,
- h_s – granular hardness,
- σ_{kk} – mean stress,
- f_d – density factor,
- d_{50} – mean grain diameter,
- a_c – micro-polar constant,
- e_c – critical void ratio (e_{c0} – value of e_c for $\sigma_{kk} = 0$),
- e_d – void ratio at maximum densification (e_{d0} – value of e_d for $\sigma_{kk} = 0$),
- e_i – maximum void ratio (e_{i0} – value of e_i for $\sigma_{kk} = 0$),
- α – pycnotropy coefficient,

n – compression coefficient,

β – stiffness coefficient,

a_1 – parameter representing the deviatoric part of the normalized stress in critical states,

ϕ_c – critical angle of internal friction during stationary flow,

θ – Lode angle.

The changes of the values of e_i, e_d and e_c decreasing with the pressure σ_{kk} according to the exponential functions (Eqs. 15–17) are shown in Fig. 3. The parameter a_1^{-1} is equal to 3.0–4.3 for the usual critical friction angles of granulates.

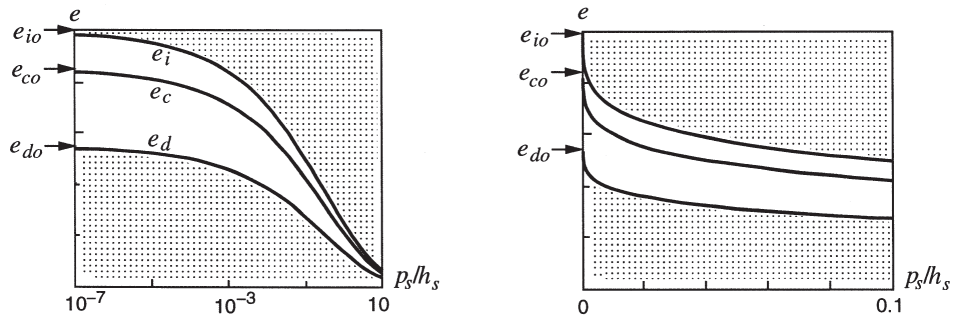

Fig. 3. Relationship between void ratios e_i, e_c and e_d and mean pressure p_s in a semi-logarithmic (a) and linear (b) scale (gray zones denote inadmissible states)

The constitutive relationship requires the following ten material constants: e_{i0}, e_{d0}, e_{c0}, ϕ_c, h_s, β, n , α, a_c and d_{50}. An exact calibration procedure of first 8 constants was given by (Herle and Gudehus 1999). The granulate hardness h_s is a density-independent reference pressure and is related to the entire skeleton (not to single grains). The granular hardness h_s and compression parameter n are estimated from a single oedometric compression test with an initially loose specimen (h_s reflects the slope of the curve in a semi-logarithmic representation, and n its curvature, Fig. 4). The constants α and β are found from a triaxial or plane strain test with a dense specimen and trigger the magnitude and position of the peak friction angle. The angle ϕ_c is determined from the angle of repose or measured in a triaxial test with a loose specimen. The values of e_{i0}, e_{d0}, e_{c0} and d_{50} are obtained with conventional index tests ($e_{c0} \approx e_{\max}, e_{d0} \approx e_{\min}, e_{i0} \approx 1.1$–$1.5\ e_{\max}$). A micro-polar parameter a_c can be correlated with the grain roughness with the aid of a numerical analysis for shearing of a narrow granular strip between two very rough boundaries (Tejchman and Gudehus 2001). It can be connected to the parameter a_1^{-1} (e.g. $a_c = 1.0 \times a_1^{-1}$). In this case, the function $N_i^c = 1.0 a_1 \hat{m}_i$ (Eq. 6).

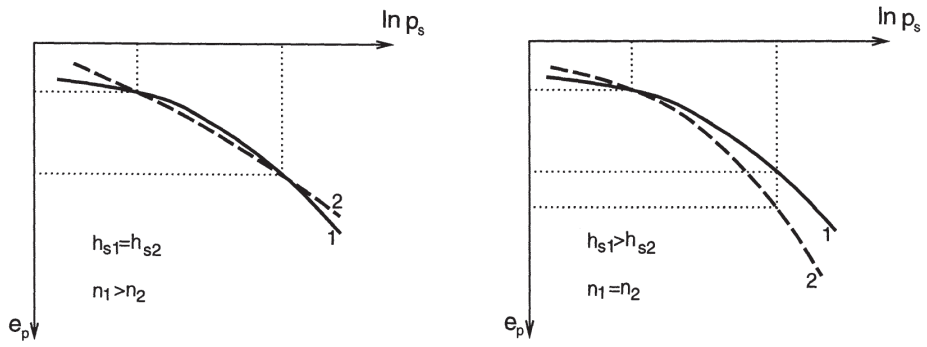

Fig. 4. Influence of n and h_s on compression curves for two different materials (p_s – mean pressure)

4. Micro-Polar Hypoplastic Model for Anisotropic Materials

The experiments (Fig. 2) show that the initial material stiffness depends on textural anisotropy. Therefore, in order to take this into account, the granular hardness h_s, which affects directly the stiffness factor in Eq. 18, was modified in the following way:

$$\bar{h}_s = h_s(1 + c \times a), \tag{24}$$

wherein c and a are the additional material parameters. The parameter a takes into account the deviatoric stress inclination with respect to the orientation in the physical space (Niemunis 2003)

$$a = \vec{M}_{ij} \overset{\wedge}{\sigma}{}^{*}_{ij}. \tag{25}$$

In turn, the tensor $\overset{\wedge}{\sigma}{}^{*}_{ij}$ stands for the deviator of the normalized stress tensor (Eq. 7) and the tensor $\vec{M}_{ij}$ is described by the expression (Niemunis 2003)

$$\vec{M}_{ij} = M_{ij} \Big/ \sqrt{M_{kl} M_{kl}} \quad \text{with} \quad M_{ij} = s_i s_j. \tag{26}$$

The tensor M_{ij} represents the dyadic product of the normal unit vector of the bedding plane (Fig. 5) with a bedding angle $\theta = 90^\circ - \delta$

$$s = [-\sin\theta, \cos\theta, 0]. \tag{27}$$

The components of the tensor M_{ij} (defining the space orientation of the symmetry plane) are

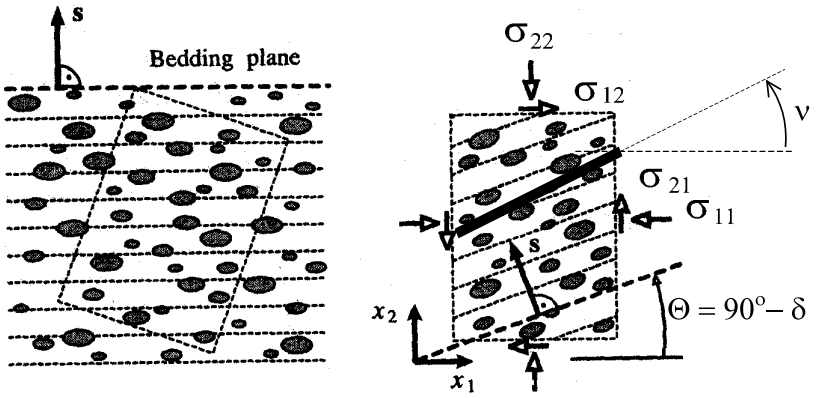

Fig. 5. Normal vector s of the bedding plane (a) and its inclination θ (b) with respect to a fixed co-ordinate system (θ – bedding plane inclination, υ – shear zone inclination)

$$\begin{bmatrix} \sin^2\theta & -\sin\theta\cos\theta & 0 \\ -\sin\theta\cos\theta & \cos^2\theta & 0 \\ 0 & 0 & 0 \end{bmatrix}. \tag{28}$$

Assuming that anisotropic effects vanish for large deformations at residual state, the evolution of the parameter c was taken as

$$c = c_1 \exp(-c_2\zeta), \tag{29}$$

wherein the parameter ζ

$$\zeta = \int \sqrt{d^c_{ij} d^c_{ij} + k_i k_i d^2_{50}}\, dt \tag{30}$$

is the length of the deformation path and c_i are two constants: c_1 (influencing the magnitude of anisotropy) and c_2 (influencing the rate of softening). The tensor d^c_{k2} denotes the rate of polar deformation and vector k_i is the rate of curvatures (Eq. 12). Using Eq. 24, the same granular hardness is approached locally at large deformations (e.g. within shear zones) whereas the average granular hardness remains anisotropic. For $\zeta = 0, c = c_1$, and for $\zeta \to \infty, c = 0$.

The FE-analyses were carried out with the material constants for so-called Karlsruhe sand: $e_{i0} = 1.30$, $e_{d0} = 0.51$, $e_{c0} = 0.82$, $\phi_c = 30^\circ$, $h_s = 190$ MPa, $\beta = 1$, $n = 0.40$, $\alpha = 0.20$, $a_c = 1.0 \times a_1^{-1}$ and $d_{50} = 0.5$ mm. In turn, the anizotropic constants c_i were assumed to be $c_1 = 1.0$ and $c_2 = 5.0$ on the basis of initial calculations. For $c_1 = 1.0$, the difference between the peak internal friction angles at $\theta = 0^\circ$ and $\theta = 90^\circ$ is about 5%–10%. In turn, for the constant $c_2 = 5.0$ (the

parameter $\zeta \approx 1$ in the shear zone at large deformations), the constant c in Eq. 29 becomes insignificant.

5. FE-data

FE-calculations of plane strain compression tests were performed with a sand specimen which was $h = 14$ cm high and $b = 4$ cm wide (similarly as in the experiments of Vardoulakis (1980)). In total, 896 quadrilateral elements (0.25×0.25 cm^2) divided into 3584 triangular elements were used. The height of the finite elements was not larger than five times mean grain diameter to properly capture shear localization. The integration was performed with one sampling point placed in the middle of each element.

A quasi-static deformation in sand was imposed through a constant vertical displacement increment Δu prescribed at nodes along the upper edge of the specimen. The boundary conditions of the sand specimen implied no shear stress at the smooth top and smooth bottom. To preserve the stability of the specimen against horizontal sliding, the node in the middle of the top edge was kept fixed. The vertical displacement increments were chosen as $\Delta u/h = 0.00005$. 8000 steps were performed.

As the initial stress state, a K_0-state with $\sigma_{22} = \gamma_d x_2$ and $\sigma_{11} = K_0 \gamma_d x_2$ was assumed in the specimen; x_2 is the vertical coordinate measured from the top of the specimen, γ_d denotes the initial volume weight and $K_0 = 0.50$ is the earth pressure coefficient at rest (σ_{11} – horizontal normal stress, σ_{22} – vertical normal stress). Next, the confining pressure $\sigma_c = 200$ kPa was prescribed.

The calculations were carried out with a uniform initial void ratio or with two different stochastic distributions of void ratio (using a normal Gauss distribution and a distribution with an exponential frequency function following Shahinpoor (1981) and Nübel and Karcher (1998)). In the case of the normal distribution, a polar form of the so-called Box-Muller transformation (1958) was used. One assumed the mean value of void ratio $\bar{e}_0 = 0.60$ with a standard deviation 0.04 and a cut-off ± 0.4. In the latter case, the spatially fluctuating initial void ratio e was calculated for individual finite elements from the formula given by Shahinpoor (1981)

$$e = -\frac{1}{\lambda} \ln \left[(1 - r) \exp(-\lambda e_m) + r \exp(-\lambda e_M) \right], \tag{31}$$

wherein the parameters are: $\lambda = 1.0$ (for a mean void ratio $\bar{e}_0 = 0.60$), $e_m = 0.001$ and $e_M = 1.64$. The random number r is chosen between 0 and 1. Eq. 31 has been derived analogously to the partition function of statistical mechanics, imposing bounds e_m and e_M upon the size of the individual Voronoi cells however. The deviation of the distribution of void ratio increases with decreasing number of voids (grains) in a volume element and decreasing mean global void ratio of the

specimen. Since the area of each finite element was $5d_{50} \times 5d_{50}$ in 2D-calculations, the initial void ratio in each element was assumed as the mean value of 25 random values calculated by Eq. 31. In all cases, the initial void ratio was limited by the pressure-dependent void ratios e_i (Eq. 15) and e_d (Eq. 16).

For the solution of a non-linear system, a modified Newton-Raphson scheme with line search was used with a global stiffness matrix calculated with only first terms of the constitutive equations (Eqs. 1). The stiffness matrix was updated every 100 steps. To accelerate the calculations in the softening regime, the initial increments of displacements and Cosserat rotations in each calculation step were assumed to be equal to the final increments in the previous step. The procedure was found to yield a sufficiently accurate and fast convergence. The magnitude of the maximum out-of-balance force at the end of each calculation step was less than 2% of the calculated total vertical force along the top of the granular specimen. Due to the presence of non-linear terms taking into the direction of the deformation rate and material softening, this procedure turned out to be more efficient than the full Newton-Raphson method. The iteration steps were performed using translational and rotational convergence criteria. For the time integration of stresses in finite elements, a one-step Euler forward scheme was applied.

The calculations were carried out with large deformations and curvatures using the so-called "Updated Lagrangian" formulation due to their effect on the results (Tejchman 2004).

6. FE-results

6.1. Stochastic Distribution of Initial Void Ratio

The numerical results for 3 different bedding plane orientations θ with a stochastic distribution of the initial void ratio of $\bar{e}_0 = 0.60$ (according to the Gauss and Shahinpoor distribution) are depicted in Figs. 6–8. The load-displacement curves are shown in Fig. 6 (P – resultant vertical force on the top, $b = 0.04$ m – specimen width, u_2 – vertical displacement of the top, $h = 0.14$ m – initial height of the sand body, $l = 1.0$ m). In turn, Fig. 7 shows the deformed FE-meshes with the distribution of the equivalent total strain $\bar{\varepsilon} = \sqrt{\varepsilon_{ij}\varepsilon_{ij}}$ at residual state ($u_2/h = 0.107$). In Fig. 8, the evolution of the equivalent total strain in specimen before and after the peak is described. The darker the region, the higher $\bar{\varepsilon}$. The entire range of the strain measure was divided into 20 different shadows, respectively.

Similarly, as in the experiments (Section 2), the vertical force on the top edge is the largest for $\theta = 0^\circ$ and smallest for $\theta = 90^\circ$. The peak overall internal friction angle calculated with the aid of principle stresses $\sigma_1 = P/(bl)$ and $\sigma_2 = \sigma_c$

$$\phi = \arcsin \frac{\sigma_1 - \sigma_2}{\sigma_1 + \sigma_2} \tag{32}$$

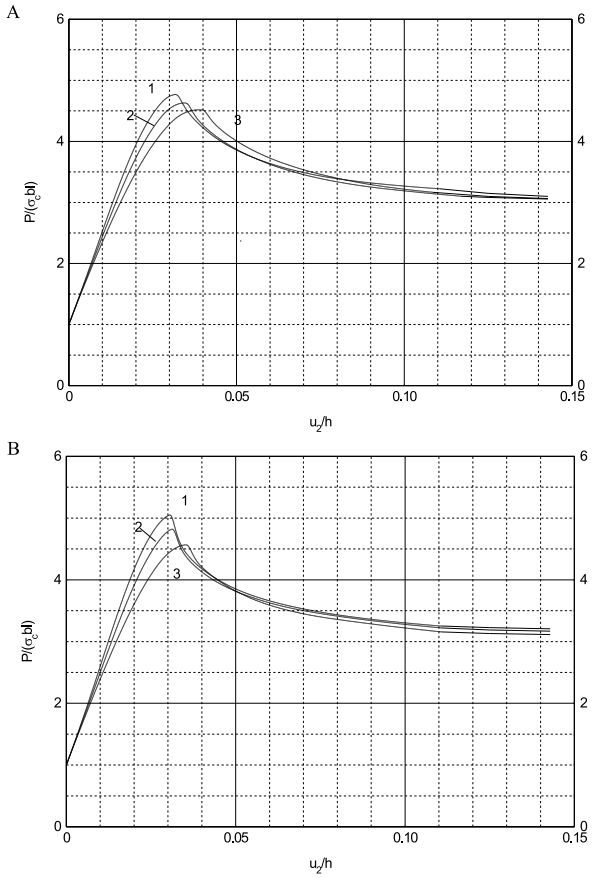

Fig. 6. Effect of the bedding plane inclination θ of Fig. 5 on the normalized load-displacement curve with $\bar{e}_0 = 0.60$: A) Gauss distribution, B) Shahinpoor distribution: 1. $\theta = 0^0$, 2. $\theta = 45^\circ$, 3. $\theta = 90^\circ$

changes between 39.6 ($\theta = 90^\circ$), 40.1° ($\theta = 45^\circ$) and 40.8° ($\theta = 0^\circ$) using the Gauss distribution and 39.8° ($\theta = 90^\circ$), 41.0° ($\theta = 45^\circ$) and 42.0° ($\theta = 0^\circ$) using the Shahinpoor distribution ($\sigma_1 = P/(bl)$, $\sigma_2 = \sigma_c$), respectively. The residual friction angle is the same, i.e. 31.5°–32.0°. The vertical strain corresponding to the peak increases with increasing θ (from $u_2/h = 0.032$ for $\theta = 0^\circ$, $u_2/h = 0.034$ for $\theta = 45^\circ$ and up to $u_2/h = 0.039$ for $\theta = 90^\circ$ using the Gauss distribution, and from $u_2/h = 0.030$ for $\theta = 0^\circ$, $u_2/h = 0.031$ for $\theta = 45^\circ$ and up to $u_2/h = 0.035$ for $\theta = 90^\circ$ using the Shahinpoor distribution).

One shear zone occurs inside the specimen which crosses it and whose location is induced by a stochastic distribution of the initial void ratio (Fig. 7). The thickness on the basis of shear deformation and modulus of deformation decreases from about 8.5 mm ($17 \times d_{50}$) for $\theta = 0^\circ$ down to 8.0 mm ($16 \times d_{50}$) for $\theta = 90^\circ$ for the Gauss distribution and from about 8.0 mm ($16 \times d_{50}$) for $\theta = 0^\circ$ down to 7.5 mm

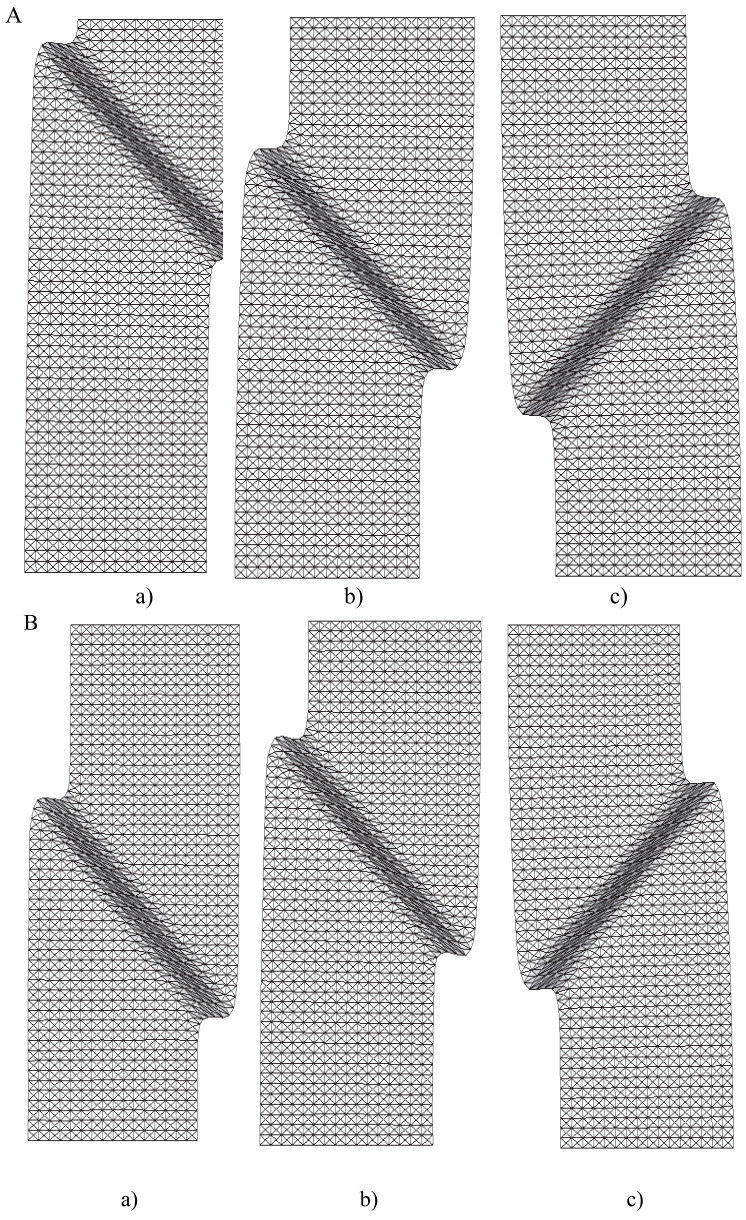

Fig. 7. Deformed meshes with the distribution of equivalent total strain $\overline{\varepsilon} = \sqrt{\varepsilon_{ij}\varepsilon_{ij}}$ at residual state at $u_2/h = 0.11$ with $\bar{e}_0 = 0.60$**:** A) Gauss distribution, B) Shahinpoor distribution, a) $\theta = 0^\circ$, b) $\theta = 45^\circ$, c) $\theta = 90^\circ$

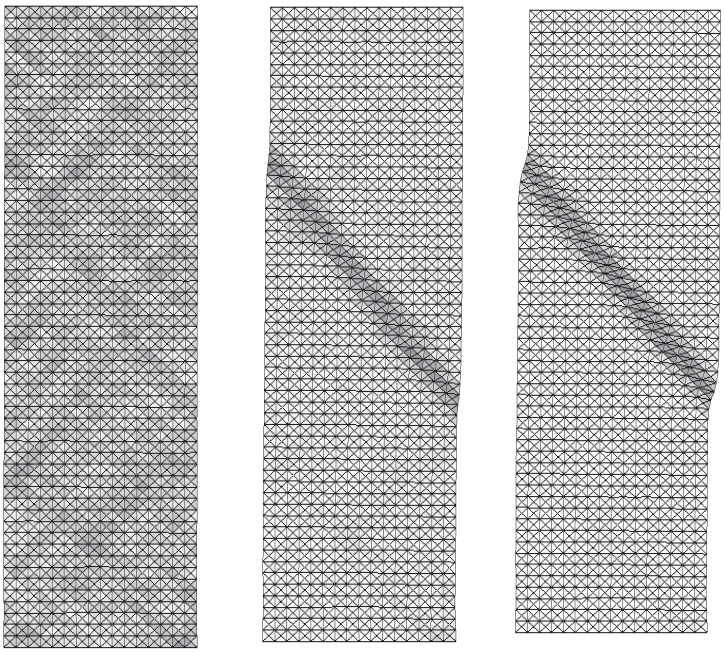

Fig. 8. Deformed mesh with the distribution of equivalent total strain $\overline{\varepsilon} = \sqrt{\varepsilon_{ij}\varepsilon_{ij}}$ at: a) $u_2/h = 0.027$, b) $u_2/h = 0.036$, c) $u_2/h = 0.045$ (Shahinpoor distribution of e_0 with $\overline{e}_0 = 0.60$, $\theta = 45^\circ$)

$(15 \times d_{50})$ for $\theta = 90^\circ$ for the Shahinpoor distribution. In turn, the inclination against the bottom decreases from about 52° ($\theta = 0^\circ$) down to 49° ($\theta = 90^\circ$). However, in the experiments (Abelev and Lade 2003), a more significant decrease of the shear zone inclination was observed (from 55° for $\theta = 0^\circ$ down to 45° for $\theta = 90^\circ$). During initial deformation, a pattern of shear zones can first be observed (Fig. 8). Next, strain localization continues to localize within a single zone.

6.2. Uniform Distribution of Initial Void Ratio

The normalized load-displacement curves for different bedding plane orientations θ with the initial uniform void ratio of $e_0 = 0.60$ and $e_0 = 0.70$ are shown in Figs. 9 and 12, respectively. No weak element was introduced to trigger shear localization. The deformed FE-mesh with the distribution of the equivalent total strain $\overline{\varepsilon}$ at residual state and before and after the peak is demonstrated in Figs. 10, 11 and 13, respectively.

In this case, the vertical force on the top edge increases with decreasing bedding angle as well. The vertical strain corresponding to the maximum vertical force also increases with increasing bedding angle. The effect of anisotropy decreases with increasing initial void ratio. The peak internal friction angles lie between

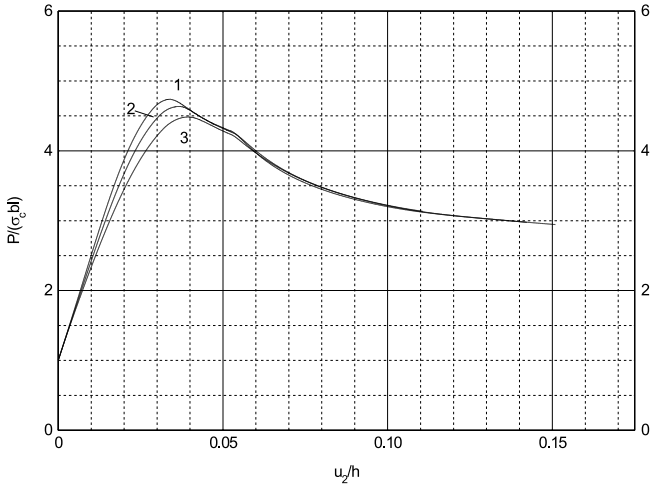

Fig. 9. Effect of the bedding plane inclination θ of Fig. 5 on the normalized load-displacement curve (uniform distribution of e_0 =0.60): 1. $\theta = 0^\circ$, 2. $\theta = 45^\circ$, 3. $\theta = 90^\circ$

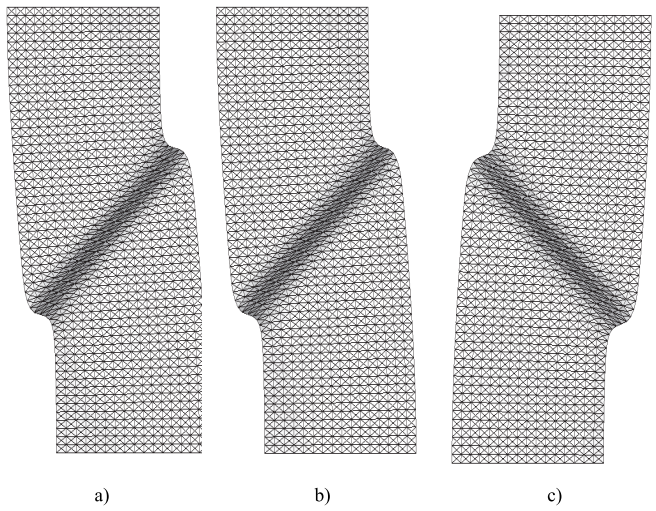

Fig. 10. Deformed meshes with the distribution of equivalent total strain $\bar{\varepsilon} = \sqrt{\varepsilon_{ij}\varepsilon_{ij}}$ at residual state at $u_2/h = 0.11$ (uniform distribution of $e_0 = 0.60$)**:** a) $\theta = 0^\circ$, b) $\theta = 45^\circ$, c) $\theta = 90^\circ$

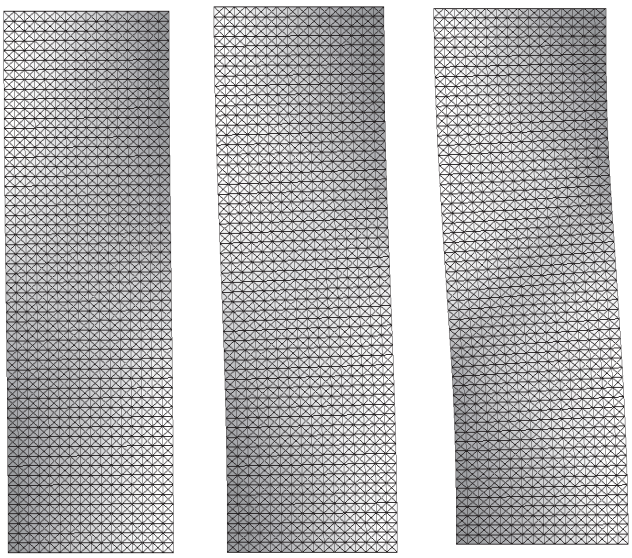

Fig. 11. Deformed mesh with the distribution of equivalent total strain $\bar{\varepsilon} = \sqrt{\varepsilon_{ij}\varepsilon_{ij}}$ at: a) $u_2/h = 0.036$, b) $u_2/h = 0.045$, c) $u_2/h = 0.054$ (uniform distribution of $e_0 = 0.60$, $\theta = 45^\circ$)

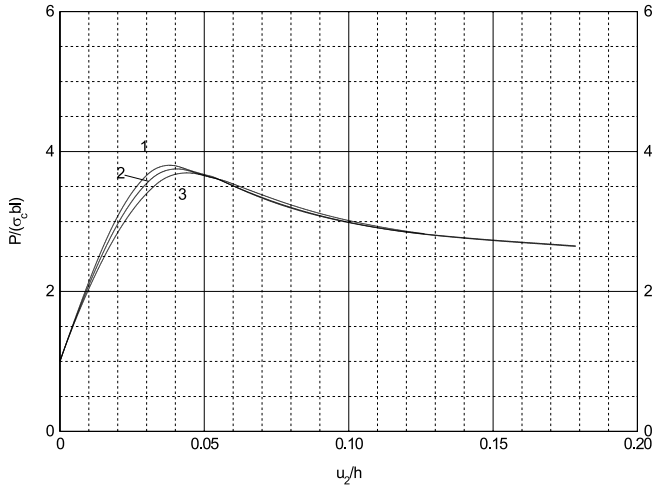

Fig. 12. Effect of the bedding plane inclination θ of Fig. 5 on the normalized load-displacement curve (uniform distribution of $e_0 = 0.70$): 1. $\theta = 0^\circ$, 2. $\theta = 45^\circ$, 3) $\theta = 90^\circ$

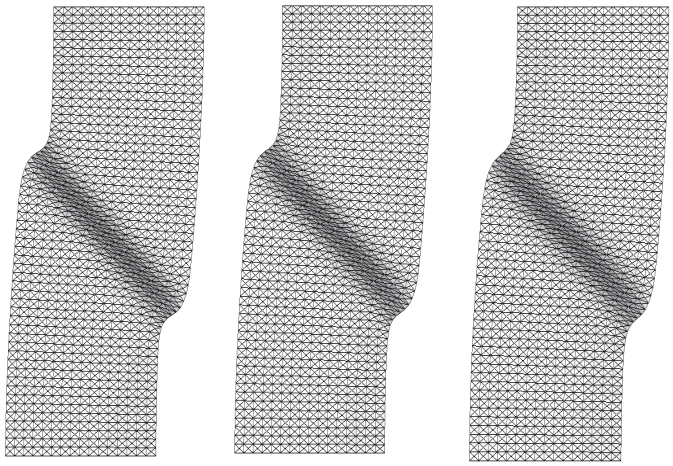

Fig. 13. Deformed meshes with the distribution of equivalent total strain $\bar{\varepsilon} = \sqrt{\varepsilon_{ij}\varepsilon_{ij}}$ at residual state at $u_2/h = 0.11$ (uniform distribution of $e_0 = 0.70$)**:** a) $\theta = 0^\circ$, b) $\theta = 45^\circ$, c) $\theta = 90^\circ$

39.4°-40.6° ($e_0 = 0.60$) and 35.0°–35.7° ($e_0 = 0.70$). They are slightly smaller than those calculated with stochastic distributions of the initial void ratio (Fig. 6).

One shear zone occurs inside of the specimen although a uniform initial void ratio was assumed. It is always located at mid-region of the specimen. The shear zone thickness slightly decreases with increasing angle θ; from about 8.0 mm ($16 \times d_{50}$) down to 7.5 mm ($15 \times d_{50}$) for $\theta = 90^\circ$ in the case of $e_0 = 0.60$, and is about 10 mm ($20 \times d_{50}$) in the case of $e_0 = 0.70$. In turn, the inclination against the bottom decreases from 50° ($\theta = 0^\circ$) down to 47° ($\theta = 90^\circ$) for $e_0 = 0.60$, and is about 47° for $e_0 = 0.70$.

The formation of shear localization is completely different in the initial phase (Fig. 11) as compared to the results with a stochastic distribution of the initial void ratio (Fig. 8). The shear localization initially develops simultaneously at the left lower corner and at the right top corner. Next, an inclined shear zone occurs in the middle of the specimen combining two regions developing further to reach a final position.

The effect of the initial void ratio is depicted in Figs. 12 and 13. The larger the initial void ratio, the smaller the effect of anisotropy on the results. The shear zone thickness (about $20 \times d_{50}$) and shear zone inclination (about 48°) are practically not influenced by the orientation of the bedding angle.

7. Conclusions

The following conclusions can be derived on the basis of FE-calculations of plane strain compression with the hypoplastic constitutive model enhanced by

micro-polar terms to capture shear localization and with the modified granular hardness to describe texturial anisotropy:

- The anisotropic effect vanishes at residual state.
- The larger the bedding plane inclination, the smaller the peak internal friction angle.
- The vertical strain corresponding to the peak on the load-displacement curve increases with the bedding plane orientation.
- The shear zone thickness decreases slightly with increasing bedding plane inclination.
- The shear zone inclination decreases with increasing bedding plane inclination.
- The position of the shear zone depends strongly on the distribution of the initial void ratio. In the case of the uniform distribution of the initial void ratio, the shear zone is always located at mid-region.
- The initial formation of shear localization strongly depends on the fact of if the initial void ratio is distributed stochastically or uniformly.
- The peak internal friction angles are slightly larger when using a stochastic distribution of the initial void ratio.
- The effect of anisotropy on shear localization decreases with increasing initial void ratio.

The FE-analyses will be continued. A careful calibration procedure of material constants will be performed to obtain a quantitative agreement with experiments (e.g. by Tatsuoka et al 1994). The calculations will be carried out for other rate boundary value problems involving shear localization. The distribution of the initial void ratio will be assumed to be spatially correlated (Walukiewicz. et al 1997).

References

Abelev A. V., Lade P. V. (2003), Effects of cross anisotropy on 3-dimensional behaviour of sand. II: Stress-strain behaviour and shear banding, *J. Eng. Mech. ASCE*, 129, 2, 167–174.

Aifantis E. C. (1984), On the microstructural origin of certain inelastic models, *J. Eng. Mater. Technol.*, 106, 326–334.

Arthur J. R. F., Phillips A. B. (1975), Homogeneous and layered sand in triaxial compression, *Geotechnique,* 25, 4, 799–815.

Bauer E. (1996), Calibration of a comprehensive hypoplastic model for granular materials, *Soils and Foundations,* 36, 1, 13–26.

Bauer E., Huang W., Wu W. (2004), Investigations of shear banding in an anisotropic hypoplastic material, *Int. J. Solids and Structures*, 41, 5903–5919.

Boehler J. P., Sawczuk A. (1977), On yielding of oriented solids, *Acta Mechanica*, 27, 185–206.

de Borst R., Mühlhaus H.-B. (1992), Gradient dependent plasticity: formulation and algorithmic aspects, *Int. J. Numer. Methods Engng.*, 35, 521–539.

de Borst R., Mühlhaus H.-B., Pamin J., Sluys L. (1992), Computational modelling of localization of deformation, *Proc. of the 3rd Int. Conf. Comp. Plasticity*, [in:] D. R. J. Owen, H. Onate, E. Hinton, eds., Swansea, Pineridge Press, 483–508.

Box G. E. P., Muller M. E. (1958), A note of the generation of random normal deviates, *Annals. Math. Stat.*, V 29, 610–611.

Chambon R. (2001), Incremental behaviour of a simple deviatoric constitutive CLoE model, *Bifurcation and Localisation Theory in Geomechanics* (eds.: Mühlhaus H.-B. et al), Swets and Zeitlinger, Lisse, 21–28.

Groen A. E. (1997), *Three-Dimensional Elasto-Plastic Analysis of Soils*, PhD Thesis, Delft University.

Gudehus G. (1986), A comprehensive constitutive equation for granular materials, *Soils and Foundations*, 36, 1, 1–12.

Gudehus G. (1997), Attractors, percolation thresholds and phase limits of granular soils, *Powder and Grains* (eds.: Behringer and Jenkins), 169–183.

Gudehus G., Nübel K. (2004), Evolution of shear bands in sand, *Geotechnique*, 54, 3, 187–201.

Herle I., Gudehus G. (1999), Determination of parameters of a hypoplastic constitutive model from properties of grain assemblies, *Mechanics of Cohesive-Frictional Materials*, 4, 5, 461–486.

Kanatani K. I. (1984), Distribution of directional data and fabric tensor, *Int. J. Engng. Science*, 22, 149–160.

Khidas Y., Jia X. (2005), Acoustic Measurements of Anisotropic Elasticity in Glass Beads Packings, [in:] *Powders and Grains* (eds.: Garcia-Rojo, Herrmann and McNamara), Taylor and Francis Group, London, 309–312.

Kolymbas D. (1977), A rate-dependent constitutive equation for soils, *Mech. Res. Comm.*, 6, 367–372.

Lade P. V. (1977), Elasto-plastic stress-strain theory for cohesionless soil with curved yield surfaces, *Int. J. Solid Structures*, 13, 1019–1035.

Lam W. K., Tatsuoka F. (1988), Effect of initial anisotropic fabric and on strength and deformation characteristics of sand, *Soils and Foundations*, 28, 1, 89–106.

Lanier J., Caillerie D., Chambon R. (2004), A general formulation of hypoplasticity, *Int. J. Numer. Anal. Methods in Geomech.*, 28, 15, 1461–1478.

Larsson J., Larsson R. (2000), Finite-element analysis of localization of deformation and fluid pressure in elastoplastic porous medium, *Int. J. Solids and Structures*, 37, 7231–7257.

Lodygowski T., Perzyna P. (1997), Numerical modelling of localized fracture of inelastic solids in dynamic loading process, *Int. J. Num. Meth. Eng.*, 40, 22, 4137–4158.

Loret B., Prevost J. H. (1990), Dynamic strain localisation in elasto-visco-plastic solids, Part 1. General formulation and one-dimensional examples, *Comp. Appl. Mech. Eng.*, 83, 247–273.

Maier T. (2002), *Numerische Modellierung der Entfestigung im Rahmen der Hypoplastizität*, PhD Thesis, University of Dortmund.

Mühlhaus H.-B. (1990), Continuum models for layered and blocky rock, *Comprehensive Rock Engineering* ([in:] J. A. Hudson,Ch. Fairhurst, editors), 2, 209–231, Pergamon Press.

Niemunis A. (2003), Anisotropic effects in hypoplasticity, *Proc. Int. Symp. on Deformation Characteristics of Geomaterials,* Lyon, France, 1, 1211–1217.

Nübel K., Karcher C. (1998), FE simulations of granular material with a given frequency distribution of voids as initial condition, *Granular Matter*, 1, 3, 105–112.

Oda M., Nemat-Nasser, Konishi J. (1985), Stress induced anisotropy in granular masses, *Soils and Foundations*, 25, 3, 85–97.

Pamin J. (1994), *Gradient-Dependent Plasticity in Numerical Simulation of Localisation Phenomena*, PhD Thesis, Delft University.

Pena A. A., Herrmann H. J., Lizcano A., Alonso-Marroquin F. (2005), Investigation of the asymptotic states of granular materials using a discrete model of anisotropic particles, [in:] *Powders and Grains* (eds.: Garcia-Rojo, Herrmann and McNamara), Taylor and Francis Group, London, 697–700.

Pestana J. M., Whittle A. J. (1999), Formulation of a unified constitutive model for clays and sands, *In. J. Num. Anal. Meth. Geomech.*, 23, 1215–1243.

Pijaudier-Cabot G., Bazant Z. P. (1987), Nonlocal damage theory, *ASCE J. Eng. Mech.*, 113, 1512–1533.

Regueiro R. A., Borja R. I. (2001), Plane strain finite element analysis of pressure sensitive plasticity with strong discontinuity, *Int. J. Solids and Structures*, 38, 21, 3647–3672.

Shahinpoor M. (1981), Statistical mechanical considerations on storing bulk solids, *Bulk Solid Handling*, 1, 1, 31–36.

Sluys L. Y. (1992), *Wave propagation, localisation and dispersion in softening solids*, PhD Thesis, Delft University of Technology.

Tatsuoka F., Nakamura S., Huang C., Tani K. (1990), Strength anisotropy and shear band direction in plane strain tests of sand, *Soils and Foundations*, 30, 1, 35–54.

Tatsuoka F., Okahara M., Tanaka T., Tani K., Morimoto T., Siddiquee M. S. (1991), Progressive failure and particle size effect in bearing capacity of footing on sand, *Proc. of the ASCE Geotechnical Engineering Congress*, 27, 2, 788–802.

Tatsuoka F., Siddiquee M. S. A., Yoshida T., Park C. S., Kamegai Y., Goto S., Kohata Y. (1994), *Testing Methods and Results of Element Tests and Testing Conditions of Plane Strain Model Bearing Capacity Tests using Air-Dried Dense Silver Leighton Buzzard Sand*, Internal Report of the Tokyo University.

Tatsuoka F., Goto S., Tanaka T., Tani K., Kimura Y. (1997), Particle size effects on bearing capacity of footing on granular material, *Deformation and Progressive Failure in Geomechanics* (eds.: A. Asaoka, T. Adachi and F. Oka), Pergamon, 133–138.

Tejchman J., Herle I., Wehr J. (1999), FE-studies on the influence of initial void ratio, pressure level and mean grain diameter on shear localisation, *Int. J. Num. Anal. Meth. Geomech.*, 23, 2045–2074.

Tejchman J., Gudehus G. (2001), Shearing of a narrow granular strip with polar quantities, *J. Num. and Anal. Methods in Geomechanics*, 25, 1–18.

Tejchman J. (2004), Influence of a characteristic length on shear zone thickness in hypoplasticity with different enhancements, *Computers and Geotechnics*, 31, 8, 595–611.

Tejchman J., Bauer E. (2005), FE-simulations of a direct and a true simple shear stress within a polar hypoplasticity, *Computers and Geotechnics*, 21, 1, 1–16.

Tejchman J., Bauer E., Wu W. (2006), Effect of texturial anisotropy on shear localization in sand during plane strain compression (under preparation).

Tejchman J., Niemunis A. (2005), FE-studies on shear localization in an anisotropic micro-polar hypoplastic granular material, *Granular Matter* (submitted for publication).

Walukiewicz H., Bielewicz E., Gorski J. (1997), Simulation of nonhomegeneous random fields for structural applications, *Computers and Structures*, 64, 1–4, 491–498.

Vardoulakis I. (1980), Shear band inclination and shear modulus in biaxial tests, *Int. J. Num. Anal. Meth. Geomech.*, 4, 103–119.

Vermeer P. (1982), A five-constant model unifying well-established concepts, *Proc. Int. Workshop on Constitutive Relations for Soils* (eds. G. Gudehus, F. Darve, I. Vardoulakis), Balkema, 175–197.

Yamada Y., Ishihara K. (1979), Anisotropic deformation characteristics of sand under three dimensional stress conditions, *Soils and Foundations*, 19, 2, 79–94.